Mechanical Characterization of Human Prostate

Steve Hwang, Mechanical Engineering

Advisor: Dr. Ellen Arruda

ABSTRACT:

Prostate fibrosis is a potential but unexplored mechanism that may contribute to the development of Lower Urinary Tract Symptoms, a disease common in aging man. The lack of mechanical studies on the prostate, however, limits our understanding on the biomechanics of the disease. It is in fact a challenge to accurately mathematically model most soft tissues because they are known to be hyperelastic and viscoelastic. This study implements the Arrua-Boyce hyperelastic model, which reflects the physics of macroscopic deformation from microscopic components. The constitutive law is fit onto experimental data to realize material parameters. The material parameters are then used on a prostate finite-element model with a simplified geometry to simulate deformation conditions. Experimental results indicate that prostate tissue is indeed hyperelastic and viscoelastic. At lower strain levels it is difficult to capture the behavior of the tissue by only using the Arruda-Boyce function given in ABAQUS, the commercial finite element modeling program used. The unloading curves are not modeled because the viscoelasticity is not included in the modeling at this point. Future work will focus on improvements by implementing a viscoelastic function and by creating a more realistically dimensioned finite element model of the prostate. Diseased prostate data will also be collected and used for modeling.

INTRODUCTION:

The lack of mechanical studies on the prostate gland limits the advancement of our understanding on the relation between various diseases and biomechanical properties of the prostate. Various analysis on the prostate have been made via magnetic resonance imaging (MRI) [4] , or needle insertion [5] , but none of them have been able to accurately capture the complex biomechanical material properties of the prostate. The major challenge at the moment is to find an accurate mathematical description of the prostate tissue. This is known to be true for most soft tissues due to nonlinear viscoelastic material properties when they undergo large mechanical deformation.

The general approach in this research project is to first select an appropriate constitutive model, in this case the Arruda-Boyce constitutive model, and then find out the material parameters of prostate. The parameters are first estimated and then realized by fitting mathematical expressions to experimental data. Those data are collected by uniaxial tensioning of prostate tissue samples under controlled testing conditions. With correct material parameters, a finite-element model of the prostate could then be used to simulate the organ's response to different conditions, including ones not possible to experimentally measure. The results of this study would be used to access the validity of applying the Arruda-Boyce model to prostate tissue, and serve as the basis for the further development of more realistic finite element models of the prostate.

BACKGROUND:

The prostate is an exocrine gland that is part of the male reproductive system. It stores and secrets a slightly alkaline fluid constituting approximately 20% of semen volume. [8] The alkalinity helps neutralize the acidity of the vaginal track, prolonging sperm survival. It includes some smooth muscles that aid in semen ejaculation, and is approximately the size of a kiwifruit, 24cc in volume. [6]

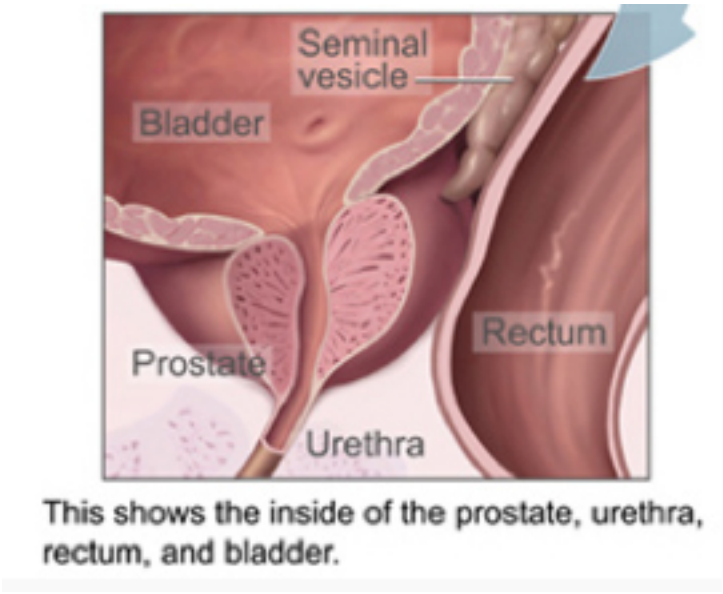

Figure 1. Prostate and surrounding organs [8]

Prostatic fibrosis, common in aging men, is one potential but unexplored mechanism that may contribute to the development and progression of Lower Urinary Tract Symptoms (LUTS). Symptoms of LUTS include urgency, nocturia, urinary frequency, weak urinary stream, and

incomplete bladder emptying. As recently reviewed by Lamborde and McVary (10), Lower Urinary Tract Symptoms (LUTS) is a progressive disorder manifest as urgency, nocturia, urinary frequency, weak urinary stream, and incomplete bladder emptying. Without effective treatment, LUTS can lead to bladder outlet obstruction and subsequent bladder wall hypertrophy, increased bladder mass, and bladder dysfunction manifest as acute urinary retention, recurrent urinary tract infections, bladder stones and, eventually, renal dysfunction. LUTS is clearly a disease of aging, and various longitudinal and population based studies have reported that the incidence and prevalence of LUTS increases concordant with age among men in the United States and worldwide (11-15).

Therefore, there is profound interest in building finite element models that could accurately reproduce the biomechanical properties of the prostate gland. The models could help relate tissue material conditions to diseases symptoms.

METHODS:

Tissue procurement and preparation

Tissue was obtained post mortem from a prostate resected at autopsy from a 66 year old male deceased from chronic lymphocytic leukemia. The patient had been taking the prescribed alpha 1-adrenergic receptor blocker, Flomax, at 0.4 mg/day and 5-alpha-reductase inhibitor, Avodart, at 0.5 mg/day, suggesting a history of LUTS. The entire prostate was received in 10% RPMI media within 24 hr of the patient's death. Upon receipt, the prostate was opened along the urethra and 9 slices of tissue were taken parallel to the urethra from one hyperplastic nodule and 9 slices were taken perpendicular to the urethra from the opposite nodule.

Mechanical testing

Mechanical testing is done in a fashion as previously described. [9][19] The 9 slices of tissue taken parallel and 9 taken perpendicular to the urethra were trimmed to equivalent volumes and dimensions of 12.3±1.7mm by 3.5±.4mm by 3.3±0.4mm, and then subjected to uniaxial load-unload mechanical testing.

These studies utilized a tensile tester custom-built in the Arruda laboratory that is constructed around a Nikon SMZ 800 dissecting microscope outfitted with a Basler A102fc digital video camera. Dual actuators are driven by stepper motors and mounted on crossed roller slides. This enables the specimen to stay in the center of view and allows for the determination of

true strain. A custom force transducer, designed to have a resolution of 50 mN, is mounted on one of the crossheads. Grips machined out of stainless steel are placed at the end of both actuators. The specimen is first gripped on each end with a micro artery clamp, which does minimal damage to the tissue but is able to withstand loading. Then the artery clamp is placed in the larger grips. The stainless steel grips are hung into a trough, submerging the specimen in saline. 25 μm diameter glass beads were brushed onto the surface of the specimen as fiduciary markers. Uniaxial servomotors and data acquisition are controlled using LabVIEW. The tissue samples are loaded at a constant true strain rate until failure, and synchronized force and image recordings are compiled using LabVIEW. The force data are converted to nominal stress by dividing by the original cross sectional area. The image data were processed using Metamorph software to track the displacements of the fiduciary markers on the specimen and convert the displacements to nominal strain. The terminal slope of the nominal stress vs. nominal strain response is the tangent modulus, or passive stiffness, of the prostate tissue in kilopascals (kPa), which is the International System of Units measure for pressure, stress, tangent modulus, and tensile strength, and is expressed as force per unit area.

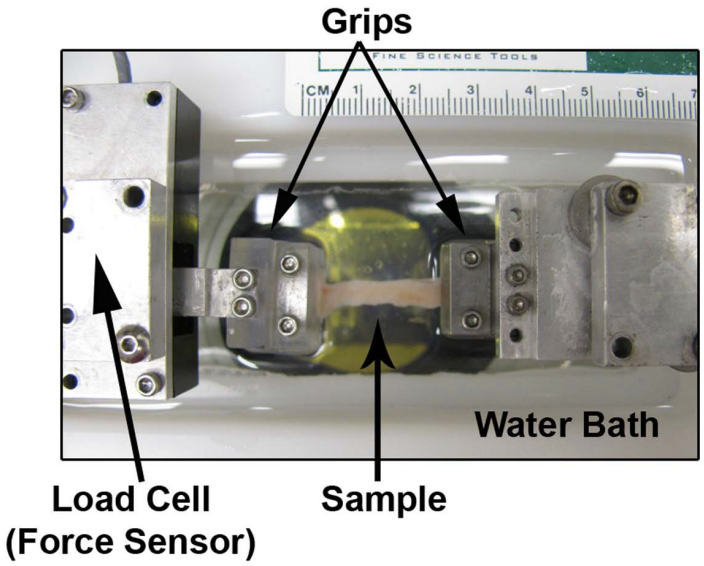

Figure 2. Uniaxial tensioning of prostate specimen

The Arrua-Boyce Constitutive Model

Soft tissues are complex engineering materials which are known to be anisotropic, non-linear, and viscoelastic [2]. The Arruda-Boyce hyperelastic constitutive model reflects the physics of macroscopic deformation from microscopic components. The model is based on Langevin chain statistics to model a material cube with eight chains in the diagonal directions. It is ideal

for soft tissues because the chains mimic collagen and elastic fibers; the tissues' main constituents. [1]

A form of the Arruda-Boyce strain energy function, very similar to the original representation, uses fifth-order series expansion of the inverse Langevin function. It does not capture the correct behavior of chain stretch approaches the limiting chain stretch, but difference between the mathematically correct implementation and the series expansion is small in most conditions. [17]

$$U = \mu\left\{\frac{1}{2}(\bar{I}_1 - 3) + \frac{1}{20\lambda_m^2}(\bar{I}_1^2 - 9) + \frac{11}{1050\lambda_m^4}(\bar{I}_1^3 - 27) + \frac{19}{7000\lambda_m^6}(\bar{I}_1^4 - 81) + \frac{519}{673750\lambda_m^8}(\bar{I}_1^5 - 243)\right\} + \frac{1}{D}\left(\frac{J_{el}^2 - 1}{2} - \ln J_{el}\right), \quad [18]$$

$$\bar{I}_1 = \bar{\lambda}_1^2 + \bar{\lambda}_2^2 + \bar{\lambda}_3^2,$$

$$\mu_0 = \mu\left(1 + \frac{3}{5\lambda_m^2} + \frac{99}{175\lambda_m^4} + \frac{513}{875\lambda_m^6} + \frac{42039}{67375\lambda_m^8}\right).$$

$$K_0 = \frac{2}{D}.$$

U is the strain energy per unit of volume. μ_0 is the initial shear modulus. I_1 is the first deviatoric strain. J_{el} is the elastic volume ratio. $\lambda_i$are the principal stretches. λ_m is the locking stretch. D is related to the material bulk modulus K_0. The material parameters used in ABAQUS, the commercial FEM program used for the project, are μ_0, λ_m, and D.

The initial shear modulus can be estimated from the initial Young's modulus, which we obtain from the average of stress-strain data from mechanical testing. We start with an estimation of $\mu_0 = E/3$ since the tissue material is assumed to be incompressible. The bulk modulus cannot be obtained from simple uniaxial testing, but it is good approximation to take it to be 100 to 1000 times larger than the shear modulus. [17]. The locking stretch could be obtained from the limiting chain stretch λ_{lim}, where the stress starts to increases without limit. [17] However, the tissue samples tend to rip before the limiting chain stretch is reached. We start with an estimation of 1.05 and 1.01 in reference to previous study. [1]

Applying Constitutive Model to FEM

Using commercial finite-element software ABAQUS, a simple model was created to simulate the uniaxial mechanical testing for prostate tissue samples. (Figure 3) Dimensions of 16mm by 4mm by 4mm were used. Appropriate boundary conditions and the same experimental strain rate of 0.01/sec were applied. The model was created under the simplified assumption of tissue being homogeneous and isotropic.

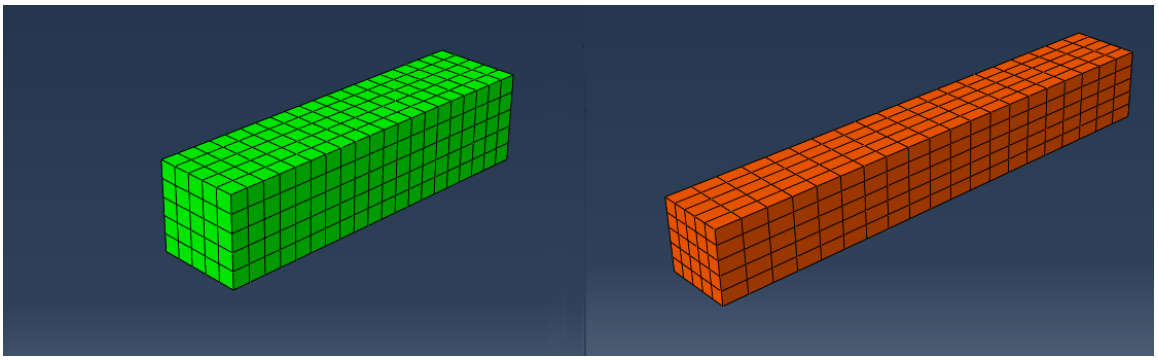

Figure 3. Prostate specimen model upstretched (left) and stretched (right). The red color on right indicates uniform distribution of stress

A range of material parameters were initially used for simulations. $\mu_0 = [20, 30, 40, 60,$ 100kPA], $\lambda_m = [1.05, 1.01, 1.001, 1.0001]$, and D=[1E-6, 1E-7, 1E-8]. Combinations of parameters were applied, and finite-element stress-strain curves were output from the simulation results and compared to results of tissue mechanical testing. Parameters were then varied through trial and error to bring simulation output closer to that of the average mechanical testing data.
A simple, cylindrical model of the entire prostate was also created. By reference to previous studies [6][7], approximate prostate volume is 24 cc, length 3.6cm, and urethra diameter 0.7 cm. The model is created as a cylinder of 3.6 cm diameter and 2.6cm thick; approximately 26.5cc in volume, with a 0.7cm diameter channel running through to represent the prostatic urethra. By implementing appropriate material parameters and then applying load or creating deformation on the inner urethra, we could observe reactions of the urethra and the surrounding tissue under different conditions.

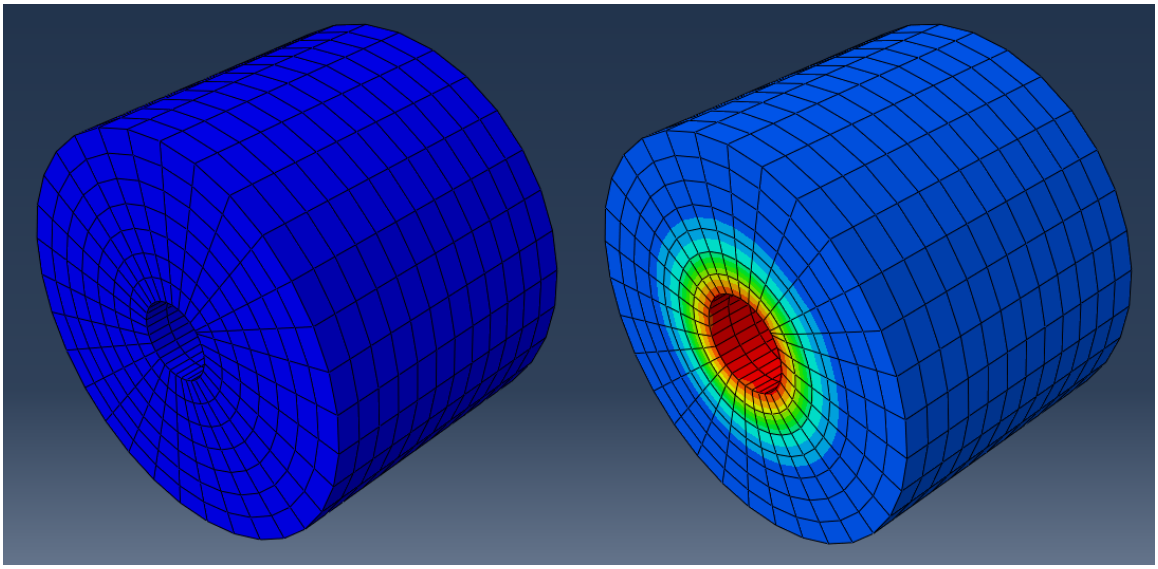

Figure 4. Simple prostate model. Without pressure applied in urethra (left) and with pressure applied. The color gradient indicates the distribution of max. principal strain throughout the model, with red being the highest and blue the lowest.

RESULTS:

Data from uniaxial mechanical testing of prostate tissue specimens show that the prostate is indeed hyperelastic and viscoelastic. (Figure 5) In order to achieve proximity in curvature to that of the average test data, the material parameters D and λ_m need to be as small as possible within the reasonable range. It was found that it does not make significant difference from D=0.001 to 0.0001, and λ_m doesn't make significant difference going smaller beyond 1E-7. The best result, shown in Figure 7, is $\mu_0 = 33kPa, \lambda_m = 1.001, \mathrm{D} = 1\mathrm{E} - 8$.

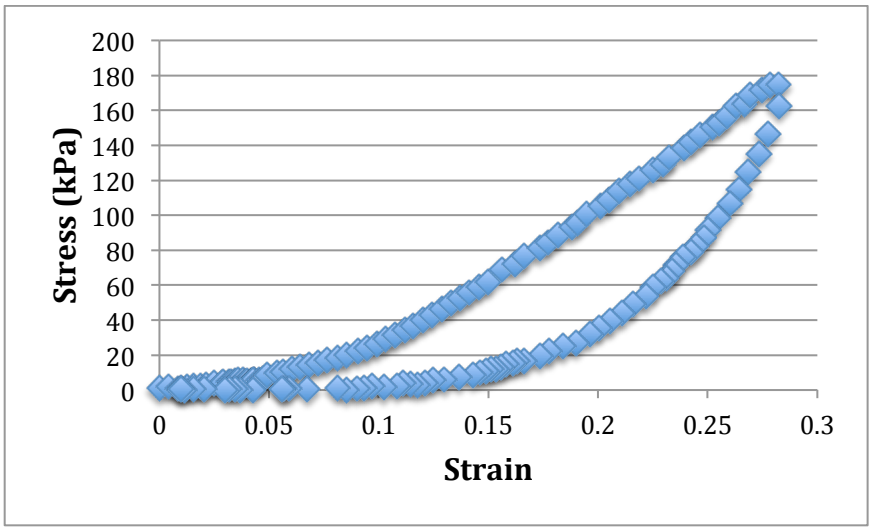

Figure 5. Stress-strain curves from uniaxial loading (top) and unloading (bottom) of prostate specimen.

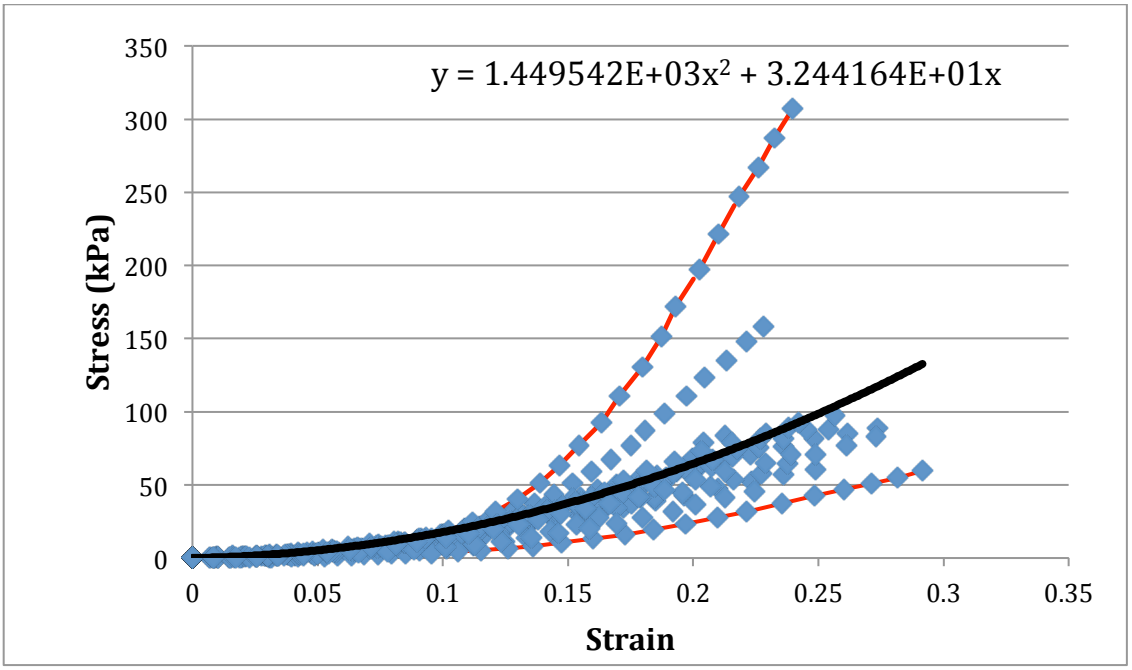

Figure 6. Test data are fit with a 2nd degree polynomial equation (black line) and used as experimental average. Top and bottom ranges are fit with red lines.

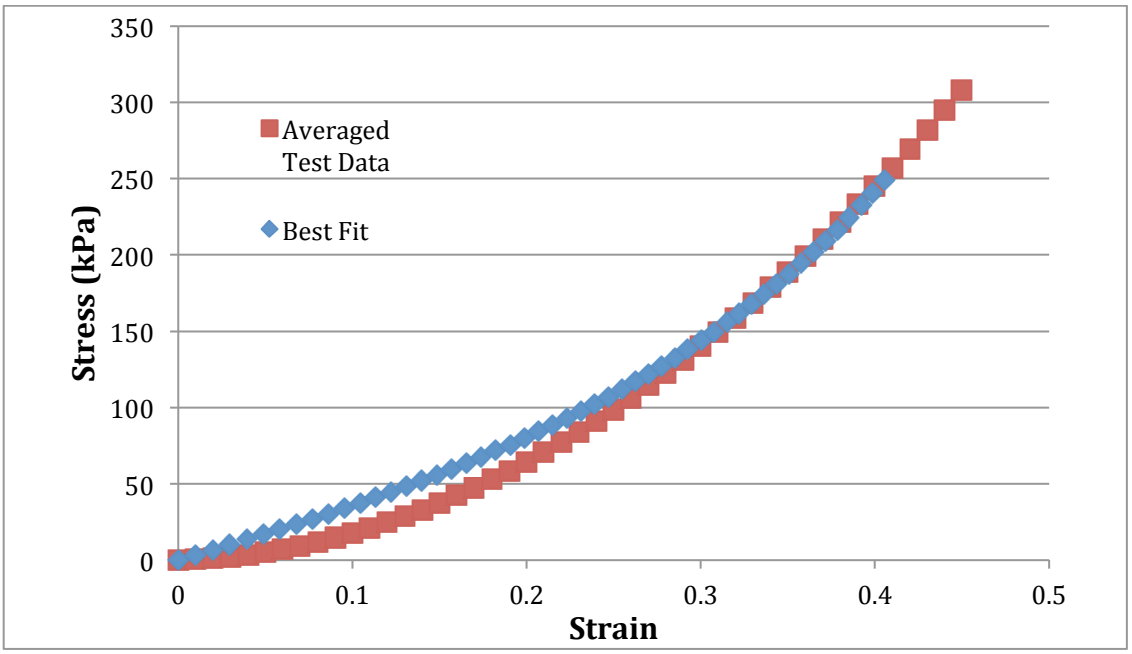

Figure 7. Averaged test data and the best fit, with material parameters $\mu_0 = 33kPa, \lambda_m = 1.001, D = 1E-8$.

DISCUSSION:

The current model is not enough to accurately reflect the biomechanical property of the prostate. As seen in Figure 7, it is difficult to realize the curvature at lower strain levels of approximately 0 to 0.15. This may possibly be because of the great amount of hysteresis found in the material, as indicated by the large area between the loading and the unloading curves. (Figure 5). The current Arruda-Boyce function in ABAQUS does not allow viscoelastic analysis. A viscoelastic mathematical model, such as the standard solid model, needs to be implemented to improve our overall modeling. Writing a user-defined function for ABAQUS to implement such a model is a goal that needs to be worked on.

In order to model a diseased prostate, we will test diseased prostate samples in the near future. Similar mechanical testing and analysis procedures will be used to procure stress-strain data, and then realize tissue material parameters. We expect the diseased model to react with less deformation to the same amount of pressure applied, since diseased prostate tissue is expected to be stiffer than healthy normal prostate tissue. By comparing the reactions of a healthy and a diseased model, we should be able to observe the effect that prostate fibrosis has on prostate flexibility and relate that to urinary disease symptoms.

Improvement on the shape of the whole prostate model could also be made. The cylindrical model is appropriate for analyzing stress-strain responses of tissue around the urethra. However, a more accurate representation of the prostate needs to be created to include geometrical effects. MRI pictures could be used to reconstruct a more accurate model in the future.

REFERENCES:

1. Liu Y, Kerdok AE, Howe RD. A Nonlinear Finite Element Model of Soft Tissue Indentation. *In Proceedings of Medical Simulation:International Symposium-ISMS* (2004), p.67.
2. Bischoff JE, Arruda EM, Grosh K. Finite Element Simulations of Orthotropic Hyperelasticity. *Finite Elements in Anlysis and Design* **38** (2002), p.983
3. Brock KK, Nichol AM. Accuracy and Sensitivity of Finite Element Mode-based Deformable Registration of the Prostate. *Medical Physics* **35** (2008),
4. Alterovitz R, Goldberg K, Pouliot J. et al. Registration of MR Prostate Images with Biomechanical Modeling and Nonlinear Parameter Estimation. *Medical Physics* **33** (2006), p. 446
5. Krishnan AP, O'Dell WG. High-order 3D FEM of Prostate Needle Insertion Forces. *IEEE* **14** (2005), p.114
6. Kalkner KM, Kubicek G, Nilsson J, Lundell M, Levitt S, Nilsson S. Prostate Volume Determination: Differential volume measurements comapring CT and TRUS. *Radiother Oncol* **81** (2006), p.179
7. Wyczółkowski M, Prajsner A, Piasecki Z, Pawlicki B. Functional Evaluation of the Prostatic Urethra by Means of Transrectal Ultrasound.
8. What You Need to Know about Prostate Cancer, National Cancer Institute. <http://www.cancer.gov/cancertopics/wyntk/prostate/allpages#ab3d4f20-6ab9-4428-9717-067035d2e691>
9. Ma J, Goble K, Smietana M. Morphological and Functional Characteristics of Three-Dimensional Engineered Bone-Ligament-Bone Constructs Following Implantation. *J. Biomech* **131** (2009)
10. Laborde EE, McVary KT. Medical management of lower urinary tract symptoms. *Rev Urol* **11** Suppl 1 (2009), p. S19.
11. Wei JT, Calhoun E, Jacobsen SJ. Urologic diseases in America project: benign prostatic hyperplasia. *J Urol* **173** (2005), p. 1256.
12. Kupelian V, Wei JT, O'Leary MP, et al. Prevalence of lower urinary tract symptoms and effect on quality of life in a racially and ethnically diverse random sample: the Boston Area Community Health (BACH) Survey. *Arch Intern Med* **166** (2006), p. 2381.
13. Parsons JK, Bergstrom J, Silberstein J, et al. Prevalence and characteristics of lower urinary tract symptoms in men aged > or = 80 years. *Urology* **72** (2008), p. 318.
14. Irwin DE, Kopp ZS, Agatep B, et al. Worldwide prevalence estimates of lower urinary tract symptoms, overactive bladder, urinary incontinence and bladder outlet obstruction. *BJU Int* (2011).
15. Parsons JK, Wilt TJ, Wang PY, Barrett-Connor E, Bauer DC, Marshall LM. Progression of lower urinary tract symptoms in older men: a community based study. *J Uro.* **183** (2010), p. 1915.
16. Bergestrom JS. Determination of Material Parameteres for the 8-chain Model for Use with ABAQUS, LS-DYNA and ANSYS
17. 4.6.1 Hyperelastic material behavior, ABAQUS Version 6.7 Documentation
18. Ma J, Gharaee-Kermani M, Kunju L, Hollingsworth J, Adler J, Arruda EM, Macoska JA. Contribution of Prostatic Fibrosis and Tissue Rigidity to Obstructive Lower Urinary Tract Symptoms